


Dynamic characteristics of a deformable capsule in a simple shear flow

Jingtao Ma, Lincheng Xu, Fang-Bao Tian,* John Young, and Joseph C. S. Lai

School of Engineering and Information Technology, University of New South Wales, Canberra, ACT 2600, Australia (Received 29 April 2018; revised manuscript received 25 December 2018; published 7 February 2019)

The dynamic characteristics of a two-dimensional deformable capsule in a simple shear flow are studied with an immersed boundary-lattice Boltzmann method. Simulations are conducted by varying the Reynolds number (Re) from 0.0125 to 2000 and the dimensionless shear rate (G) from 0.001 to 0.5. The G - Re plane can be divided into four regions according to the deformation dependence on the parameters considered: viscous dominant, inertia dominant, transitional, and anomalous regions. There are four typical dynamic behaviors over the G - Re plane: steady deformation, prerule state, quasisteady deformation, and continuous elongation. Analysis indicates that the pressure distribution and its variations due to the interplay of the fluid inertia force, the viscous shear stress, and the membrane elastic force determines the complex behaviors of the capsule. The effects of the bending rigidity and the internal-to-external viscosity ratio on the dynamics of the capsule are further studied. It is found that the capsule experiences smaller deformation when the higher bending rigidity is included, and the low bending rigidity does not have a remarkable influence on the capsule deformation. The capsule normally experiences smaller deformation due to the increase of the internal-to-external viscosity ratio.

DOI: [10.1103/PhysRevE.99.023101](https://doi.org/10.1103/PhysRevE.99.023101)**I. INTRODUCTION**

The dynamics of a capsule enclosed by a thin elastic membrane has received rapidly growing interest due to its wide applications in many fields such as cosmetics and the pharmaceutical industry [1–3]. A typical example of a capsule is a red blood cell (RBC) which is composed of a lipid bilayer membrane encapsulating a Newtonian hemoglobin solution [4], and deformation of the RBC can significantly affect the rheology of blood and the oxygen load release [5]. Therefore, it is desirable to understand the dynamics of a capsule in flow.

A capsule immersed in a viscous shear flow can exhibit complex behaviors (e.g., tank-treading, tumbling, and swinging movements) [4,6–8]. The dynamics of a capsule in a viscous shear flow is determined by the interplay of the fluid inertia force, the viscous shear stress, and the membrane elastic force and has been studied by utilizing theoretical, experimental, and numerical methods [9–18]. Previous numerical investigations have mainly focused on the deformation of a capsule at low and moderate Reynolds numbers (e.g., $Re \leq 100$) [19–21]. The fluid inertia effects on the dynamics of a capsule in a shear flow at Reynolds numbers up to 100 were studied by Sui *et al.* [19] and Song *et al.* [20]. It was found that the fluid inertia has significant effects on the capsule transient deformation and duration as well as the flow structure around and inside the capsule when the Reynolds number is larger than 1. Krüger *et al.* [22] also reported a similar conclusion for the suspension of capsules. Bai *et al.* [21] studied a viscoelastic capsule deformation in a shear flow at Reynolds numbers ranging from 0.1 to 10. They found that the inertia can significantly affect the transient and steady-state deformation of the capsule if the Reynolds number is larger

than 0.1. Despite these studies, the underlying mechanism of the inertia effect leading to larger capsule deformation is still not well understood. In addition, the capsule dynamics in a shear flow at high Reynolds numbers (e.g., $Re > 100$) has seldom been investigated. As stated in Refs. [23,24], Reynolds numbers up to $O(10^3)$ may induce fragments of RBCs exposed to high shear stress (e.g., 250 Pa or higher) leading to the phenomenon of hemolysis (rupturing of the cell and release of the contents). It would be helpful to understand the mechanism behind hemolysis by investigating the dynamics of a capsule at high Reynolds numbers. In this paper, we study the dynamics of a two-dimensional (2D) capsule in a simple shear flow at Reynolds numbers ranging from 0.0125 to 2000 and dimensionless shear rates ranging from 0.001 to 0.5.

The organization of the paper is as follows. Section II describes the physical problem, mathematical formulation, and numerical method. The numerical results and discussion are presented in Sec. III. Finally, concluding remarks are provided in Sec. IV.

II. PHYSICAL PROBLEM AND MATHEMATICAL FORMULATION

In this paper, we numerically investigate the dynamics of a 2D capsule with an initial diameter of $2a$ in an incompressible shear flow (as demonstrated by Fig. 1). A linear shear flow is applied between the top and bottom walls. Due to the interplay of the viscous shear stress, the fluid inertia, and the capsule elastic stress, the capsule in the computational domain experiences transient deformation, and develops into an equilibrium configuration, an unsteady pattern, or an extremely stretched state depending on the values of the Reynolds number and the dimensionless shear rate.

In this work, the liquid within the capsule and the ambient fluid are assumed to be incompressible, and their dynamic

*Corresponding author: f.tian@adfa.edu.au; onetfbao@gmail.com

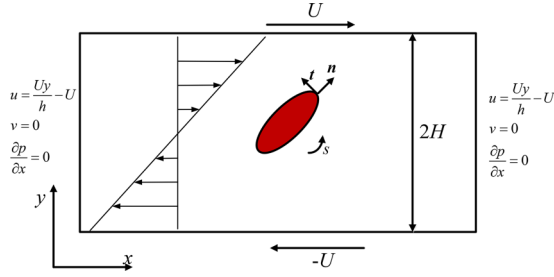
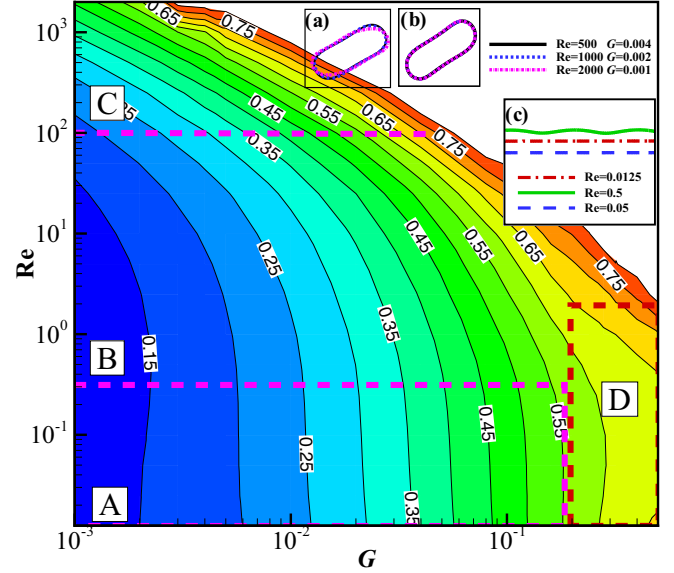


FIG. 1. Schematic illustration of a capsule in a simple shear flow.

viscosities are respectively $\lambda\mu$ and μ , where λ is the internal-to-external viscosity ratio. The dynamics of the fluids are governed by the Navier-Stokes equations $\nabla \cdot \mathbf{u} = 0$ and $\frac{\partial(\rho\mathbf{u})}{\partial t} + \nabla \cdot (\rho\mathbf{u}\mathbf{u}) = -\nabla p + \widehat{\mu}\nabla^2\mathbf{u}$, where ρ is the fluid density, \mathbf{u} is the fluid velocity, p is the pressure, and $\widehat{\mu} = \lambda\mu$ for the internal fluid and μ for the external fluid. The capsule is modeled as a membrane, and the equation describing the development of the force on the membrane is $\mathbf{F} = -\frac{\partial}{\partial s}(\tau\mathbf{t} + q\mathbf{n})$, where τ is the in-plane tension, q is the transverse shear tension, s is the arc length coordinate, \mathbf{t} is the unit tangent vector pointing to the direction of the increasing s , and \mathbf{n} is the unit normal vector pointing to the external fluid. The in-plane tension τ is obtained by $\tau = E_s(|\frac{\partial\mathbf{X}}{\partial s_0}| - 1)$, where E_s is the stretching coefficient of the capsule membrane, and \mathbf{X} is the position vector of a point on the capsule membrane. The transverse shear tension q is determined by $q = d\{E_b[\epsilon(s) - \epsilon_0(s)]\}/ds$, where E_b is the bending coefficient, $\epsilon(s)$ is the instantaneous membrane curvature, and $\epsilon_0(s)$ is the initial curvature of membrane at the minimum bending energy configuration [25]. Although we recognize the limitation of the current model (i.e., 2D and Hookean membrane), we nevertheless feel that the results obtained by this simple model will be of help in understanding the capsule dynamics, because based on the previous studies (e.g., Refs. [26–28]), the results obtained by using the 2D model show some features common with the three-dimensional (3D) simulations. In this work, we choose the flow shear rate (i.e., k), density, and the radius of the capsule to nondimensionalize the governing equations and obtain four dimensionless parameters: Reynolds number $\text{Re} = \rho(2a)^2k/\mu$, dimensionless shear rate $G = \mu ka/E_s$, dimensionless bending modulus $e_b = E_b/(a^2E_s)$, and viscosity ratio λ . Here k is defined by U/H as shown in Fig. 1. Note that Re measures the ratio of the fluid inertia to the shear stress and G represents the ratio of the shear force to the membrane elastic force. Therefore, $\text{Re}G$ can be used to measure the ratio of the inertia force to the elastic force.

In this work, the multiple-relaxation-time lattice Boltzmann method combined with the immersed boundary method [5,29–33] is used to solve the fluid-structure system. In this method, the discrete lattice Boltzmann method is utilized for simulating fluid dynamics, and the immersed boundary method is employed to deal with the effects of immersed boundary by spreading the stress exerted by the boundary onto the collocated fluid nodes near the boundary. The details of this method and its validation can be found in our previous work [5,29–31].


 FIG. 2. The contours of the mean D_{xy} on the G - Re plane. Insets (a) and (b) are profiles of the capsule at nondimensional time $kt = 12$, and 60 for high Re and low G . Inset (c) shows the time histories of D_{xy} at low Re and $G = 0.32$.

III. RESULTS AND DISCUSSION

Simulations are conducted by varying Re from 0.0125 to 2000 and G from 0.001 to 0.5. The computational domain ranges from 0 to $20a$ in both x and y directions (i.e., $H = 10a$). The mesh spacing is $\Delta x = \Delta y = 0.05a$. According to Refs. [5,19,34], such a computational domain is reasonable for this application. Validations have been performed to ensure that the numerical results are independent of mesh size. To measure the capsule deformation, the Taylor shape parameter D_{xy} is introduced [5,19,34], $D_{xy} = (L - W)/(L + W)$, where L and W are the length and width of the capsule in the shear plane, respectively. In the present research, D_{xy} ranges from 0 (nondeformation) to 1 (zero volume).

A. Effects of G and Re on the mean D_{xy} and the dynamic behaviors of the capsule

The effects of G and Re on the mean D_{xy} and the dynamic behaviors of the capsule are studied in this section. It should be noted that the bending rigidity is neglected (i.e., $e_b = 0$) and the viscosity ratio of the internal to external fluids is set to be 1 (i.e., $\lambda = 1$). The effects of bending rigidity and viscosity ratio on the capsule dynamics are studied in Secs. III B and III C, respectively.

1. Effects of G and Re on the mean D_{xy}

The contours of mean (time-averaged) D_{xy} on the G - Re plane are shown in Fig. 2, where the G - Re plane is divided into four regions based on the relationship between D_{xy} and G - Re : viscous dominant (A), transitional (B), inertia dominant (C), and anomalous (D) regions.

It is found that the increase of Re or G contributes to the increase of D_{xy} , except the region D which will be further discussed later. In region A (i.e., $\text{Re} \leq 0.3$, $G < 0.2$), D_{xy} is independent of the Reynolds number, which is consistent

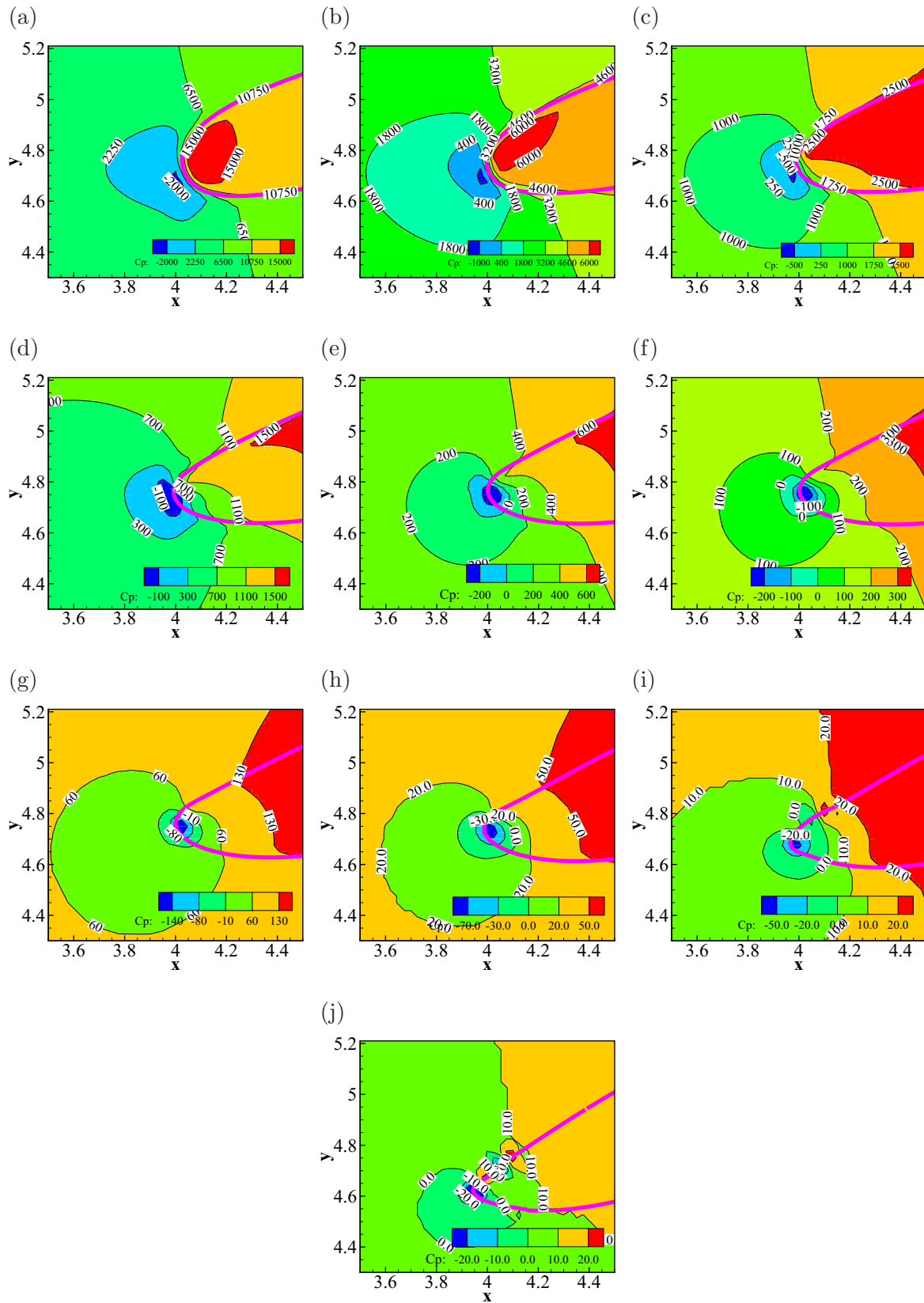


FIG. 3. The contours of the pressure coefficient at $kt = 60$ and $G = 0.32$ at different Reynolds numbers: (a) 0.001, (b) 0.0025, (c) 0.005, (d) 0.01, (e) 0.025, (f) 0.05, (g) 0.1, (h) 0.25, (i) 0.5, and (j) 1.0.

with investigations presented in Refs. [5,34]. This is understandable because at low Reynolds numbers the effects of the inertia force on the fluid motion are negligible, and the shear force to the capsule elastic force ratio, measured by G , is the only parameter governing the capsule deformation. In region C (i.e., $Re \geq 100$), D_{xy} is proportional to $Re G$. This is due to the fact that at high Reynolds numbers, the fluid-structure system is determined by the fluid inertia to the capsule elastic force ratio, measured by $Re G$. Insets (a) and (b) in Fig. 2 show the capsule profiles for three cases: (i) $Re = 500$, $G = 0.004$; (ii) $Re = 1000$, $G = 0.002$; and (iii) $Re = 2000$, $G = 0.001$, where the values of $Re G$ are the same. It can be found that the capsule profiles for three cases are the same at $kt = 60$, even though at the transient stage (e.g., $kt = 12$) the capsule deformation at $Re = 2000$ is quite different from those at the other two Reynolds numbers further confirming that the deformation of the capsule is determined by $Re G$ at higher Reynolds numbers. Region B is a transitional region where both the fluid viscous and inertia forces have an interplay effect on the capsule deformation. It is also interesting to observe a special region: region D (i.e., $G \geq 0.2$, $Re \leq 2.0$) where D_{xy} experiences a different trend from that at lower G .

To further illustrate the capsule behavior in region D, the time histories of D_{xy} at $G = 0.32$ and $Re = 0.0125$, 0.05 and 0.5 are shown in inset (c) in Fig. 2. It is found that D_{xy} drops slightly and then rises with the increase of the Reynolds number. In addition, D_{xy} is unsteady at $Re = 0.5$ for $G > 0.2$. This phenomenon of periodic oscillation of D_{xy} has been attributed to be a “numerical artifact” as discussed in Ref. [28]. To explain the behaviors of D_{xy} in region D, the distribution of the pressure coefficient [scaled by $0.5\rho(2a\kappa)^2$] contours at $G = 0.32$ and Re ranging from 0.001 to 1.0 at nondimensional time $kt = 60$ are shown in Fig. 3. At $Re = 0.001$, a lower pressure center is observed outside the capsule tip exerting a stretching force on the capsule. When Re is increased (e.g., from 0.001 to 0.025), the pressure difference across the capsule tip drops leading to a decreasing stretching force. This explains the observation that D_{xy} decreases with the increase of Re when $0.001 \leq Re \leq 0.025$. When $Re > 0.025$, the lower pressure center moves inside the capsule, and the stretching force becomes the compressing force which causes a further decrease of D_{xy} . When Re is further increased (e.g., from 0.05 to 1.0), the low pressure in the internal region increases, which results in the decreasing compressing force on the capsule. This provides a reasonable explanation for the increase of D_{xy} when Re is increased from 0.05 to 0.1 .

To further explain the inertia effect leading to larger capsule deformation, the contours of the pressure coefficient at $kt = 2$, $G = 0.01$, and $Re = 50$, 100 , 250 , and 1000 are shown in Fig. 4. Here $kt = 2$ is used, because the difference between all cases discussed is obviously initiated at this instant. For all Reynolds numbers, it is observed that there are two low pressure centers located near the capsule tips, which are caused by the effect similar to the flow around an exterior corner, and biased from the direction of the long axis of the capsule, leading to an anticlockwise moment. This anticlockwise moment exerts a resistance to the long-term elongation of the capsule. When Re increases, the pressure increases which reduces the resistance, and thus leads to a larger deformation.

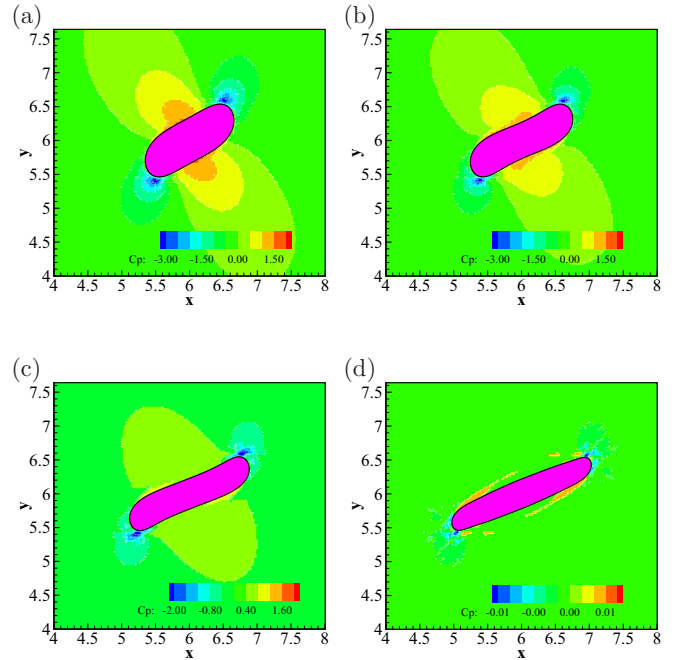


FIG. 4. The contours of the pressure coefficient at $kt = 2$ and $G = 0.01$ at different Reynolds numbers: (a) 50, (b) 100, (c) 250, (d) 1000.

2. Dynamic behaviors of the capsule

The dynamics of the capsule can be classified into four regimes as shown in Fig. 5. Please note that these four regimes are independent of the four regions discussed in Sec. III A 1. The first regime is steady deformation, where the capsule exhibits a steady shape. This regime occurs in the low D_{xy} region (i.e., small deformation). The critical D_{xy} below which the steady deformation occurs depends on Re .

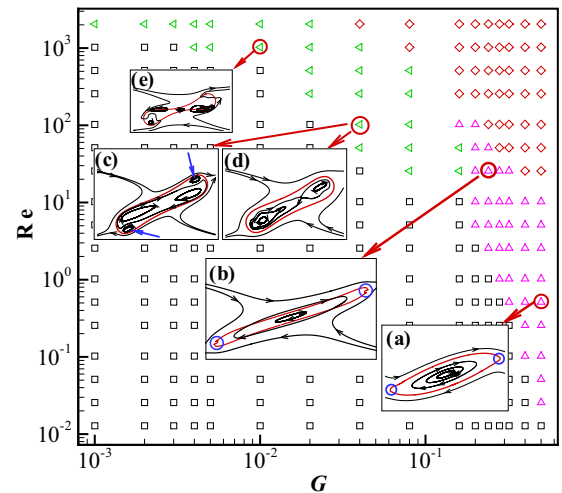


FIG. 5. The dynamic behaviors of the capsule at different Reynolds numbers and dimensionless shear rates. \square , steady deformation; \triangle , prerule state; \triangleleft , quasisteady deformation; \diamond , continuous elongation. Insets: streamline patterns around the capsule at (a) $Re = 0.5$, $G = 0.5$, $kt = 68$; (b) $Re = 25$, $G = 0.16$, $kt = 10$; (c) $Re = 100$, $G = 0.04$, $kt = 22$; (d) $Re = 100$, $G = 0.04$, $kt = 60$; and (e) $Re = 1000$, $G = 0.01$, $kt = 20$.

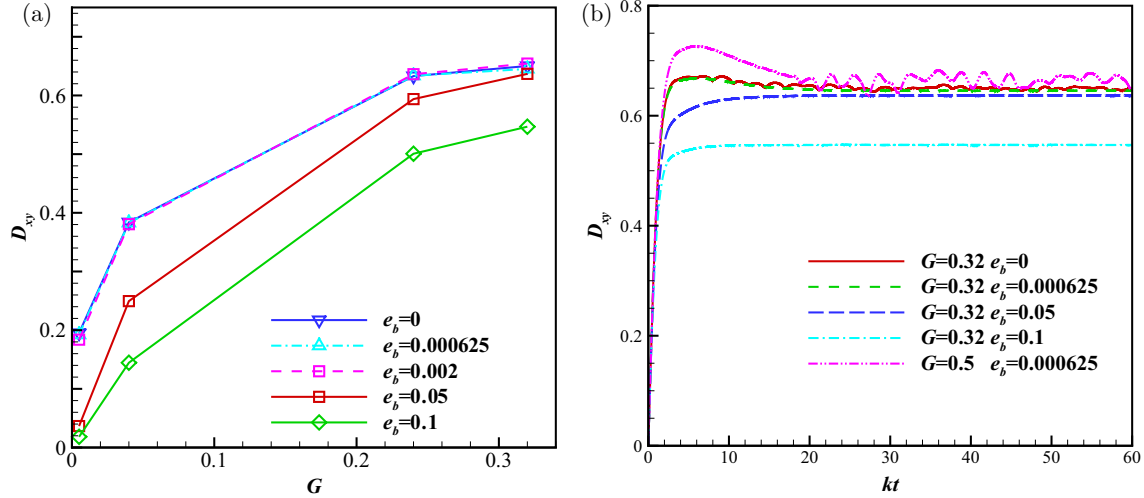


FIG. 6. (a) The relationship between the Taylor shape parameter D_{xy} and the dimensionless shear rate G at $Re = 1.0$ and $e_b = 0, 0.000625, 0.002, 0.05, 0.1$. (b) The time histories of D_{xy} at $G = 0.32$ and $e_b = 0, 0.000625, 0.05, 0.1$ and $G = 0.5$ and $e_b = 0.000625$.

Specifically, the critical D_{xy} is about 0.6 when $Re \leq 100$, and drops to below 0.45 when Re approaches 2000. The second regime is prerupture state which occurs at high G and low and moderate Re regions where D_{xy} is larger than 0.62. The sharp capsule tips with very high curvatures appear in this regime as demonstrated by insets (a) and (b) (marked by blue circles) in Fig. 5. Similar sharp tips have also been observed in previous experimental and numerical studies [35,36]. The high curvatures of the capsule tips caused the rupture of the capsule [35] and the divergence of the simulation [36]. In the present study, the high curvatures of the capsule tips do not lead to the divergence of the simulations, and they lead to two typical capsule behaviors: (i) tip oscillation and (ii) wrinkling surface. The third regime is quasisteady deformation which occurs at large Re where $0.45 < D_{xy} < 0.95$. In this regime, the capsule vibrates along its long axis direction at a very low frequency or experiences tip-oscillation motion over its long axis, which may be caused by the fluid-structure dynamics between the capsule and the fluid enclosed, as shown by insets (c)–(e) in Fig. 5. Specifically, insets (c) and (d) show the unsteady behavior associated with the secondary eddies inside the capsule (marked by blue arrows) for $Re = 100$ and $G = 0.04$. This observation is different from that reported in Ref. [19] which predicted a steady state for this case. As demonstrated by inset (e), the capsule is stretched into a dumbbell shape, and similar behavior has also been observed in the experimental study by Ref. [23]. This shape was indicated as the deformation stage preceding the rupture of the capsule, which agrees with the present study. The last regime is a continuously elongated state which occurs at large Re and large G where D_{xy} is larger than 0.9.

B. The effects of bending rigidity on the capsule dynamics

The effects of bending rigidity on the capsule dynamics are studied here. The dimensionless bending modulus e_b can be quite small (in the order of 10^{-4} to 10^{-3}) for problems involving the capsule deformation in biological systems. For example, for a RBC with the diameter of $7.8 \mu\text{m}$, the elastic and bending moduli are

respectively (6.0×10^{-6}) – $(1.2 \times 10^{-4}) \text{ N m}^{-1}$ and $2.4 \times 10^{-19} \text{ N m}$ [37,38], and the dimensionless bending modulus e_b ranges from 0.00013 to 0.0026. Here $e_b = 0.000625$ and 0.002 are used to study the effects of the low bending rigidity on the capsule deformation. In addition, it can be expected that the higher bending rigidity (i.e., e_b is higher than 10^{-3}) would alter the capsule deformation, and $e_b = 0.05$ and 0.1 are used to study the effects of the higher bending rigidity on the capsule deformation. The internal-to-external viscosity ratio is set to be 1 (i.e., $\lambda = 1$).

Figure 6(a) shows the relationship between the mean Taylor shape parameter D_{xy} and the dimensionless shear rate G at $e_b = 0, 0.000625, 0.002, 0.05, 0.1$ and $Re = 1.0$. It is found that the capsule experiences smaller deformation when the higher bending rigidity (i.e., $e_b = 0.05$ and 0.1) is included, and D_{xy} decreases with the increase of e_b . In contrast, the capsule almost experiences the same deformation as that of $e_b = 0$ (i.e., neglecting the bending effect) when the low bending rigidity is included. This means the low bending rigidity does not have a significant influence on the mean Taylor shape parameter D_{xy} of the capsule. In addition, the bending rigidity also changes the dynamic state of the capsule. For example, as shown in Fig. 6(b), D_{xy} reaches steady state at $e_b = 0.000625, 0.05, 0.1$ for $G = 0.32$, while D_{xy} experiences oscillation at $e_b = 0$. This means including the bending rigidity is helpful to stabilize the behavior of the capsule at low Reynolds numbers. However, when G increases to 0.5, the oscillation occurs again at $e_b = 0.000625$, showing that incorporating a low bending modulus which is in the range of red blood cells does not change the physics discussed in Sec. III A, but does change the regime boundaries.

C. The effects of viscosity ratio on the capsule dynamics

In this section, the effects of the viscosity ratio λ on the deformation of the capsule at two different Reynolds numbers (i.e., 1.0 and 250.0, which are respectively located in the viscosity-dominated and inertia-dominated regimes) are studied, and four different values of G are selected for each Re

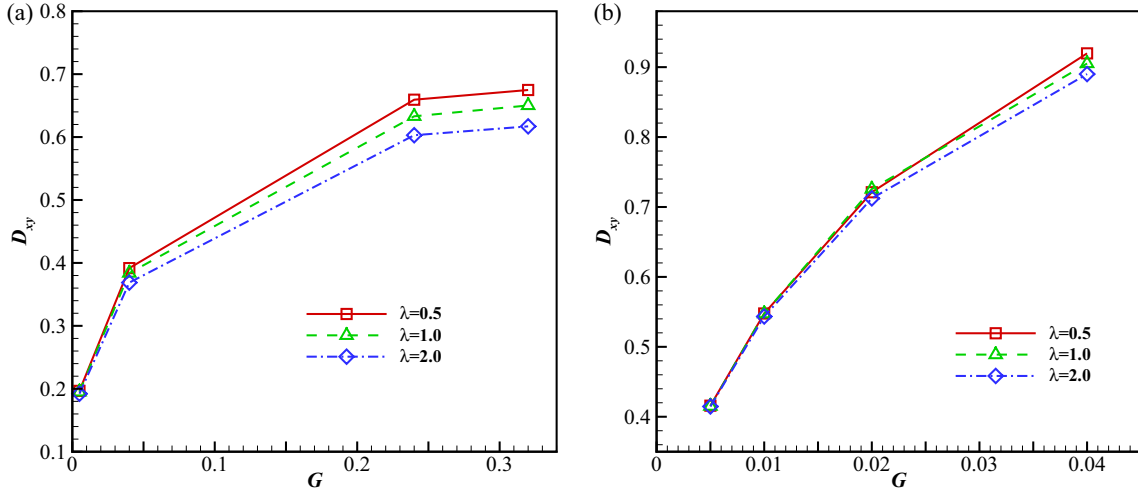


FIG. 7. The relationship between the Taylor shape parameter D_{xy} and the dimensionless shear rate G at different viscosity ratios and $Re =$ (a) 1.0 and (b) 250.

($G = 0.005, 0.04, 0.24,$ and 0.32 for $Re = 1.0$ and $G = 0.005, 0.01, 0.02,$ and 0.04 for $Re = 250.0$). The bending stiffness is neglected here.

Figure 7 shows the relationship between the Taylor shape parameter D_{xy} and the dimensionless shear rate G at viscosity ratios $\lambda = 0.5, 1.0,$ and 2.0 and $Re = 1.0$ and 250.0 . It is found that incorporating the viscosity difference between the exterior and interior regions of the capsule does not significantly change the deformation of the capsule, and thus the physics discussed in Sec. III A is repeatable within the ratios considered. In addition, D_{xy} generally decreases with the increase of the viscosity ratio λ , and the viscosity ratio λ has smaller effects on D_{xy} at smaller deformation regime than at larger deformation regime. This trend is consistent with the 3D studies by Ramanujan and Pozrikidis [39] and Foessel *et al.* [40].

D. Discussion

The Reynolds numbers considered in the present research are in the range of many biological and engineering systems. The results obtained in this paper can be used to explain phenomena observed in reality and give guidance to practical applications. For example, drug delivery by a capsule is a promising method to treat diseases such as cancer [41]. It is necessary to choose a capsule with the proper membrane characteristics to prevent vascular occlusion, especially in blood vessels with a clot. The shear rate in an artery with a clot can reach $425\,000\text{ s}^{-1}$ [42], and the corresponding shear Reynolds number is approximately 4 for a capsule with a diameter of $10\ \mu\text{m}$. In this case, it would be preferable to choose a capsule with the smaller modulus to prevent blockage of the blood vessel.

IV. CONCLUDING REMARKS

In summary, we have numerically studied the capsule deformation in a simple shear flow with the immersed boundary–lattice Boltzmann method by varying the Reynolds number from 0.0125 to 2000 and dimensionless shear rate from 0.001 to 0.5. It is found that the Taylor shape parameter

D_{xy} is independent of the Reynolds number at low Reynolds numbers ($Re \leq 0.3$) and small dimensionless shear rate G ($G < 0.2$), and is approximately proportional to ReG at higher Reynolds numbers ($Re \geq 100$). It is also observed that D_{xy} experiences a different trend at $G \geq 0.2$ and $Re \leq 2.0$ where D_{xy} first decreases and then increases when Re ranges from 0.0125 to 2.0, which is caused by the migration of the low pressure center from the external region of the capsule tip to the internal region and the increase of the low pressure in the internal region. In addition, the dynamics of the capsule can be classified into four regimes depending on the values of Re , G , and D_{xy} . In the low D_{xy} region (e.g., $D_{xy} \leq 0.6$ at $Re \leq 100$, and the critical value of D_{xy} drops to below 0.45 when Re increases to 2000), the capsule exhibits a steady shape. At low and moderate Re (e.g., $Re \leq 100$) and high G (e.g., $G \geq 0.16$), the sharp tips with very high curvatures appear, and two behaviors (tip oscillation and wrinkling surface) occur due to the high curvatures. At $Re \geq 25$ and $0.45 < D_{xy} < 0.95$, the capsule vibrates along its long-axis direction at a very low frequency or experiences tip-oscillation motion over its long axis. In the large Re and large G region (e.g., $ReG \geq 40$) and, the capsule continuously elongates. In addition, the resistance due to two low-pressure regions near the capsule tips and biased from the capsule long axis decreases when the Reynolds number increases, which is a reasonable explanation of the inertia effect at large Reynolds numbers. The effects of the bending rigidity and viscosity ratio of the internal to the external fluids on the dynamics of the capsule are also studied. It is found that the capsule tends to experience smaller deformation when the high bending rigidity is included, but the low bending rigidity does not have a significant influence on the time-averaged D_{xy} of the capsule. The bending effects tend to stabilize the capsule behaviors, but the oscillation of the capsule may occur again with the increase of G . The capsule normally experiences smaller deformation due to the increase of the viscosity ratio of the internal to the external fluids. The results in present research are helpful to explain the mechanism of the deformation of droplets, blood cells, emulsions, and capsules, especially at relatively high Reynolds numbers (e.g., $Re \geq 100$).

ACKNOWLEDGMENTS

This research is undertaken with the assistance of resources from the National Computational Infrastructure, which is supported by the Australian Government. J.M.

acknowledges the UNSW University College Postgraduate Research Scholarship during the pursuit of this study. F.-B.T. is the recipient of an Australian Research Council Discovery Early Career Researcher Award (Project No. DE160101098).

-
- [1] E. Lac, A. Morel, and D. Barthes-Biesel, *J. Fluid Mech.* **573**, 149 (2007).
- [2] Z. Y. Luo and B. F. Bai, *Phys. Fluids* **28**, 101901 (2016).
- [3] D.-V. Le and K.-H. Chiam, *Phys. Rev. E* **84**, 056322 (2011).
- [4] M. Abkarian, M. Faivre, and A. Viallat, *Phys. Rev. Lett.* **98**, 188302 (2007).
- [5] F.-B. Tian, *Comput. Math. Meth. Med.* **2016**, 7981386 (2016).
- [6] S. Kessler, R. Finken, and U. Seifert, *J. Fluid Mech.* **605**, 207 (2008).
- [7] Y. Sui, H. T. Low, Y. T. Chew, and P. Roy, *Phys. Rev. E* **77**, 016310 (2008).
- [8] J. Dupire, M. Socol, and A. Viallat, *Proc. Natl. Acad. Sci. USA* **109**, 20808 (2012).
- [9] H. Schmid-Schönbein and R. Wells, *Science* **165**, 288 (1969).
- [10] H. Goldsmith, *Biorheology* **7**, 235 (1971).
- [11] H. Goldsmith and J. Marlow, *Proc. R. Soc. London, Ser. B* **182**, 351 (1972).
- [12] T. M. Fischer, M. Stohr-Lissen, and H. Schmid-Schonbein, *Science* **202**, 894 (1978).
- [13] D. Barthes-Biesel, *J. Fluid Mech.* **100**, 831 (1980).
- [14] T. Gao, H. H. Hu, and P. P. Castañeda, *J. Fluid Mech.* **687**, 209 (2011).
- [15] Y. Sui, Y. Chew, P. Roy, Y. Cheng, and H. Low, *Phys. Fluids* **20**, 112106 (2008).
- [16] Y. Chen, X. Liu, and Y. Zhao, *Appl. Phys. Lett.* **106**, 141601 (2015).
- [17] Z. Wang, Y. Sui, P. D. M. Spelt, and W. Wang, *Phys. Rev. E* **88**, 053021 (2013).
- [18] T. Krüger, F. Varnik, and D. Raabe, *Comput. Math. Appl.* **61**, 3485 (2011).
- [19] Y. Sui, Y. Chew, P. Roy, and H. Low, *Comput. Fluids* **38**, 49 (2009).
- [20] C. Song, S. J. Shin, H. J. Sung, and K.-S. Chang, *J. Fluids Struct.* **27**, 438 (2011).
- [21] B. F. Bai, Z. Y. Luo, S. Q. Wang, L. He, T. J. Lu, and F. Xu, *Microfluid. Nanofluid.* **14**, 817 (2013).
- [22] T. Krüger, B. Kaoui, and J. Harting, *J. Fluid Mech.* **751**, 725 (2014).
- [23] S. Suter and M. Mehrjardi, *Biophys. J.* **15**, 1 (1975).
- [24] L. Leverett, J. Hellums, C. Alfrey, and E. Lynch, *Biophys. J.* **12**, 257 (1972).
- [25] Y. Sui, Y. T. Chew, P. Roy, X. B. Chen, and H. T. Low, *Phys. Rev. E* **75**, 066301 (2007).
- [26] J. Beaucourt, F. Rioual, T. Séon, T. Biben, and C. Misbah, *Phys. Rev. E* **69**, 011906 (2004).
- [27] Y. Sui, Y. Chew, and H. Low, *Int. J. Mod. Phys. C* **18**, 993 (2007).
- [28] G. Breyiannis and C. Pozrikidis, *Theor. Comput. Fluid Dyn.* **13**, 327 (2000).
- [29] F. B. Tian, H. Luo, and X. Y. Lu, *Phys. Fluids* **23**, 111903 (2011).
- [30] F. B. Tian, H. Luo, L. Zhu, and X. Y. Lu, *Phys. Rev. E* **82**, 026301 (2010).
- [31] F.-B. Tian, H. Luo, L. Zhu, J. C. Liao, and X.-Y. Lu, *J. Comput. Phys.* **230**, 7266 (2011).
- [32] F.-B. Tian, *Appl. Phys. Lett.* **103**, 034101 (2013).
- [33] D. Sun, Y. Wang, D. Jiang, N. Xiang, K. Chen, and Z. Ni, *Appl. Phys. Lett.* **103**, 071905 (2013).
- [34] T. Gao and H. H. Hu, *J. Comput. Phys.* **228**, 2132 (2009).
- [35] K.-S. Chang and W. L. Olbricht, *J. Fluid Mech.* **250**, 609 (1993).
- [36] E. Lac, D. Barthes-Biesel, N. Pelekasis, and J. Tsamopoulos, *J. Fluid Mech.* **516**, 303 (2004).
- [37] J. Zhang, P. C. Johnson, and A. S. Popel, *Phys. Biol.* **4**, 285 (2007).
- [38] D. A. Fedosov, B. Caswell, and G. E. Karniadakis, *Biophys. J.* **98**, 2215 (2010).
- [39] S. Ramanujan and C. Pozrikidis, *J. Fluid Mech.* **361**, 117 (1998).
- [40] E. Foessel, J. Walter, A.-V. Salsac, and D. Barthès-Biesel, *J. Fluid Mech.* **672**, 477 (2011).
- [41] J. B. Wolinsky, Y. L. Colson, and M. W. Grinstaff, *J. Controlled Release* **159**, 14 (2012).
- [42] D. Salac and M. J. Miksis, *J. Fluid Mech.* **711**, 122 (2012).